











RESEARCH ARTICLE | MAY 17 2024

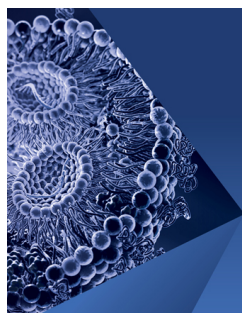
Comparison of high-order numerical methodologies for the simulation of the supersonic Taylor–Green vortex flow **FREE**

Jean-Baptiste Chapelier ; David J. Lusher ; William Van Noordt; Christoph Wenzel ; Tobias Gibis ; Pascal Mossier; Andrea Beck ; Guido Lodato ; Christoph Brehm ; Matteo Ruggeri ; Carlo Scalo ; Neil Sandham 



Physics of Fluids 36, 055146 (2024)

<https://doi.org/10.1063/5.0206359>



Physics of Fluids

Special Topic:

Flow and Lipid Nanoparticles

Guest Editors: Richard Braatz and Mona Kanso

Submit Today!

Comparison of high-order numerical methodologies for the simulation of the supersonic Taylor–Green vortex flow

Cite as: Phys. Fluids **36**, 055146 (2024); doi: [10.1063/5.0206359](https://doi.org/10.1063/5.0206359)

Submitted: 1 March 2024 · Accepted: 29 April 2024 ·

Published Online: 17 May 2024








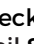






View Online



Export Citation



CrossMark

Jean-Baptiste Chapelier,^{1,a)}  David J. Lusher,^{2,b)}  William Van Noordt,^{3,c)}  Christoph Wenzel,^{4,d)} 
Tobias Gibis,^{4,e)}  Pascal Mossier,^{4,f)}  Andrea Beck,^{4,g)}  Guido Lodato,^{5,h)}  Christoph Brehm,^{6,i)} 
Matteo Ruggeri,^{7,j)}  Carlo Scalo,^{7,k)}  and Neil Sandham^{2,l)} 

AFFILIATIONS

¹ONERA—Department of Aerodynamics, Aeroelasticity and Acoustics, 92322 Châtillon, France

²Aerodynamics and Flight Mechanics Group, University of Southampton, Southampton SO17 1BJ, United Kingdom

³Department of Engineering Science, University of Oxford, Wellington Square, Oxford OX1 2JD, United Kingdom

⁴Institute of Aerodynamics and Gas Dynamics, University of Stuttgart, 70569 Stuttgart, Germany

⁵INSA Rouen Normandie—CORIA-CNRS—76800 Saint-Etienne-du-Rouvray, France

⁶Aerospace Engineering, Alfred Gessow Rotorcraft Center, University of Maryland at College Park, College Park, Maryland 20742, USA

⁷School of Mechanical Engineering, Purdue University, West Lafayette, Indiana 47906, USA

^{a)} Author to whom correspondence should be addressed: jean-baptiste.chapelier@onera.fr

^{b)} Electronic mail: d.lusher@soton.ac.uk

^{c)} Electronic mail: william.vannoordt@eng.ox.ac.uk

^{d)} Electronic mail: wenzel@iag.uni-stuttgart.de

^{e)} Electronic mail: gibis@iag.uni-stuttgart.de

^{f)} Electronic mail: pascal.mossier@iag.uni-stuttgart.de

^{g)} Electronic mail: andrea.beck@iag.uni-stuttgart.de

^{h)} Electronic mail: guido.lodato@insa-rouen.fr

ⁱ⁾ Electronic mail: cbrehm1@umd.edu

^{j)} Electronic mail: mruggeri@purdue.edu

^{k)} Electronic mail: scalo@purdue.edu

^{l)} Electronic mail: n.sandham@soton.ac.uk

ABSTRACT

This work presents a comparison of several high-order numerical methodologies for simulating shock/turbulence interactions based on the supersonic Taylor–Green vortex flow, considering a Reynolds number of 1600 and a Mach number of 1.25. The numerical schemes considered include high-order Finite Difference, Targeted Essentially Non-Oscillatory, Discontinuous Galerkin, and Spectral Difference schemes. The shock capturing methods include high-order filtering, localized artificial diffusivity, non-oscillatory numerical fluxes, and local low-order switching. The ability of the various high-order numerical methodologies to both capture shocks and represent accurately the development of turbulent vortices is assessed.

Published under an exclusive license by AIP Publishing. <https://doi.org/10.1063/5.0206359>

I. INTRODUCTION

The accurate representation of turbulent scales using high-fidelity modeling approaches such as direct numerical simulation or large-eddy simulation is particularly challenging in engineering practice due to the wide range of scales considered and their interaction with numerical

errors stemming from the discretization method. For such problems, it is customary to employ high-order numerical methods that provide low levels of numerical dissipation and dispersion, enabling an accurate representation of the small scales of turbulence. However, high-order numerical schemes are often less robust than their lower-order counterparts, posing

problems when considering stiff problems such as supersonic flows and shock waves. A number of industrial applications involve shock/turbulence interactions, such as cruising aircraft configurations or engines. In this context, it is of the utmost importance to establish numerical schemes that are robust regarding shock capturing and retain a high accuracy for the representation of the turbulent scales.

In the present paper, several of those methodologies are compared based on a canonical shock/turbulence interaction flow problem, namely, the supersonic Taylor–Green vortex. The incompressible—or low Mach—Taylor–Green vortex flow problem¹ has become a widely used test case for assessing numerical flow solvers, and in particular, their ability to characterize precisely the development of turbulence scales.^{2–5} More recently, a supersonic version of this flow problem has been introduced,⁶ which features turbulence scales progressively breaking down and their interactions with shocks, allowing as assessment of the ability of numerical methods to capture shocks, whilst still accurately representing the turbulence cascade. This case is of great interest for comparing numerical methods, as its initial condition is analytical and can be exactly reproduced in different flow solvers. The supersonic Taylor–Green vortex case has been introduced recently and, to the authors' knowledge, this is the first time a cross-comparison involving several numerical methodologies is performed for this test case. In terms of physical phenomena, it features transition, fully developed turbulence, strong shocks, and shock–turbulence interaction. The closest configuration in terms of flow physics would be compressible isotropic turbulence. This flow features small-amplitude shocks (or shocklets) interacting with turbulence and might resemble the later stages of evolution of the supersonic Taylor–Green vortex case used in the present work.⁷

In this work, established Finite Difference schemes and modern variants for shock and turbulence capturing are considered, as well as more recent Discontinuous Finite Element methods for which the treatment of such problems is still an open topic of investigation. Among the numerical methods considered, we consider Targeted Essentially Non-Oscillatory (TENO),⁸ Discontinuous Galerkin (DG),⁹ Spectral Difference (SD),^{10,11} Flux Reconstruction (FR),¹² and compact Finite Difference (FD)^{13,14} schemes. Without any specific treatment of the discontinuities, high-order solvers tend to produce oscillations around shocks, which eventually lead to nonphysical states, such as negative values of density or pressure. In this study, shock capturing is handled either by non-oscillatory numerical fluxes, high-order filters, localized artificial diffusivity (LAD) or local switching to a lower order, more robust scheme (i.e., an embedded Finite Volume TVD scheme). A mesh convergence study is conducted and the ability of each method to capture large and small turbulent scales, as well as shocks depending on the resolution, is assessed from select quantities of interest.

The paper is organized as follows. First, the governing equations and description of the Taylor–Green Vortex flow case are described in Sec. II, as well as the reference solutions and quantities of interest. Section III presents the various numerical methodologies considered in the present work. Section IV concerns the description and analysis of the results. Finally, conclusions are drawn in Sec. V.

II. GOVERNING EQUATIONS AND FLOW PROBLEM SPECIFICATION

A. Compressible Navier–Stokes equations

The compressible Navier–Stokes equations governing compressible fluid flow motion are considered, which are given as follows:

$$\frac{\partial \rho}{\partial t} + \nabla \cdot (\rho \mathbf{u}) = 0, \quad (1)$$

$$\frac{\partial \rho \mathbf{u}}{\partial t} + \nabla \cdot (\rho \mathbf{u} \otimes \mathbf{u} + p \mathbf{I} - \boldsymbol{\tau}) = 0, \quad (2)$$

$$\frac{\partial \rho E}{\partial t} + \nabla \cdot (\mathbf{u}(\rho E + p) - \boldsymbol{\tau} \cdot \mathbf{u} + \mathbf{q}) = 0, \quad (3)$$

where ρ is the density, E the total energy, \mathbf{u} is the velocity vector, $\mathbf{q} = -\lambda \nabla T$ is the heat flux, and $\boldsymbol{\tau} = \mu(\nabla \mathbf{u} + \nabla \mathbf{u}^T - \frac{2}{3}(\nabla \cdot \mathbf{u})\mathbf{I})$ is the viscous stress tensor. The dynamic viscosity is expressed as a function of temperature following Sutherland's law:

$$\mu(T) = \frac{1.4042(T/T_{\text{ref}})^{1.5}}{T/T_{\text{ref}} + 0.4042} \mu_{\text{ref}}. \quad (4)$$

The thermal conductivity is defined as $\lambda = \mu \frac{C_p}{Pr}$, with Pr the Prandtl number set to the value 0.71. The pressure is a function of the conservative variables following the ideal gas equation of state:

$$p = (\gamma - 1) \left(\rho E - \frac{1}{2} \mathbf{u} \cdot \mathbf{u} \right), \quad (5)$$

where γ is the specific heat ratio set to the value 1.4 suitable for air.

B. Taylor–Green vortex flow setup

The Taylor–Green vortex problem features the analytical initialization of large vortices in a cubic, periodic computational domain and the subsequent transition and breakdown of the initial vortices toward a turbulent state. The computational domain is a cubic box $\Omega = [-\pi L, \pi L]^3$ with periodic boundary conditions. In terms of primitive variables, the initialization features a constant temperature field and reads

$$\mathbf{u}(\mathbf{x}, t = 0) = \begin{pmatrix} U_0 \sin\left(\frac{x}{L}\right) \cos\left(\frac{y}{L}\right) \cos\left(\frac{z}{L}\right) \\ -U_0 \cos\left(\frac{x}{L}\right) \sin\left(\frac{y}{L}\right) \cos\left(\frac{z}{L}\right) \\ 0 \end{pmatrix}, \quad (6)$$

$$p(\mathbf{x}, t = 0) = p_0 + \frac{\rho_0 U_0^2}{16} \left(\cos\left(\frac{2x}{L}\right) + \cos\left(\frac{2y}{L}\right) \right) \times \left(2 + \cos\left(\frac{2z}{L}\right) \right), \quad (7)$$

$$T(\mathbf{x}, t = 0) = T_0. \quad (8)$$

Here, T_0 is set to the reference temperature T_{ref} of the Sutherland law. The Mach and Reynolds numbers are defined as $M_0 = U_0 \sqrt{\frac{\rho_0}{\gamma p_0}}$ and $Re = \frac{\rho_0 U_0}{\mu_0}$, respectively. This particular initialization features an isothermal flow field, with variations of the density and pressure in the domain. Figure 1 illustrates the vortices and density gradients relative to this flow problem at the initial time and the time $t = 10$ for which the turbulent structures have developed in the computational domain.

C. Flow diagnostics and reference solution

As flow diagnostics, we consider the time evolution of three quantities of interest, spatially integrated over the computational

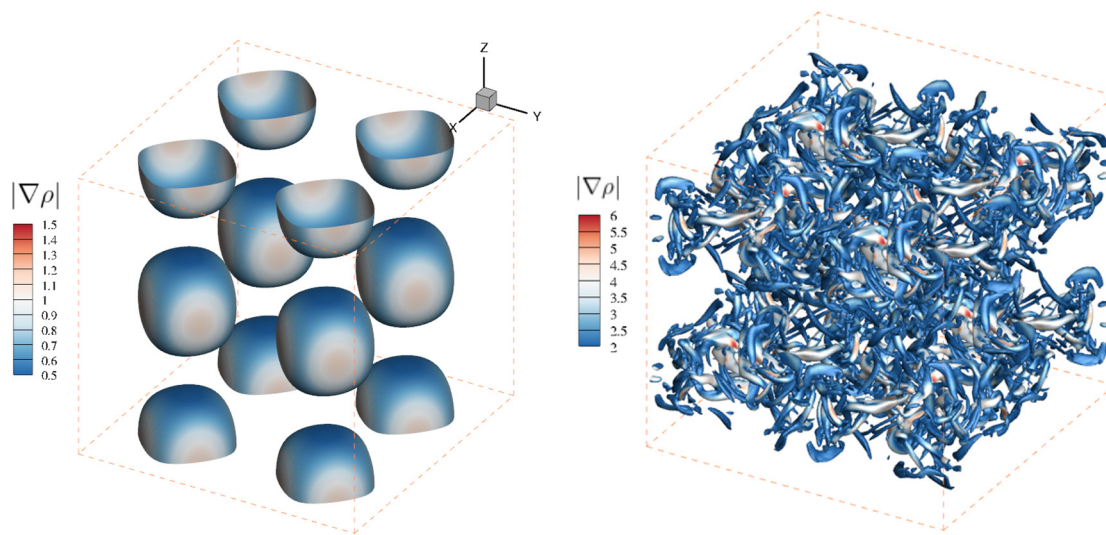


FIG. 1. TGV flow at $Re = 1600$ and $M_0 = 1.25$: Q-criterion iso-surfaces colored by the density gradient magnitude, extracted from a 256^3 degrees of freedom simulations with fourth-order of accuracy using the CODA DG solver. Left: initial condition; Right: field at $t = 10$.

domain Ω . For each quantity described, we also present a mesh convergence study of the $M_0 = 1.25/Re = 1600$ case obtained with the OpenSBLI¹⁵ solver using a sixth-order TENO scheme for consistency with the original work on this benchmark problem.⁶ TENO schemes⁸ are a fairly recent (2016) addition to the family of Essentially Non-Oscillatory (ENO) shock-capturing schemes that have been in use for several decades in high-speed CFD research. They improve upon previous ENO and Weighted Essentially Non-Oscillatory (WENO) schemes by having considerably lower numerical dissipation, while still retaining robust shock-capturing capability.⁶ These characteristics make them ideal for simulating compressible turbulence with shock-waves and, therefore, a suitable choice for providing the benchmark solutions in this work. TENO schemes achieve this behavior via a modified ENO-like staggered stencil layout, and a strong scale-separation procedure for controllable low dissipation. TENO schemes have already been applied to a wide range of complex fluid flow problems. A comprehensive review on the different variants and their applications was given in Ref. 16.

The extremely fine meshes used for the reference solutions in this study required substantial computational resources on distributed-memory supercomputing clusters. For the finest mesh solution of 2048^3 degrees of freedom (DoFs) provided by the OpenSBLI solver with a sixth-order TENO scheme, a total of 57 600 ARM-based Fujitsu A64FX CPU cores (1200 nodes, 48 CPU cores/node) were utilized. In addition to the compute requirements, the reference solutions require large amounts of disk storage and memory. With 2048^3 DoFs, each three-dimensional snapshot of the flow-field requires 520GB of storage in double precision.

While OpenSBLI is more frequently used on GPU-based machines, the flexibility of the OPS parallel library allowed us to explore a hybrid MPI+OpenMP CPU-based approach for this study instead. In total, 4800 MPI ranks were used at $N = 2048^3$ [four ranks per node, one distributed to each Core Memory Group (CMG)], with 12 OpenMP threads

on each rank. For a non-dimensional time step of $\Delta t = 2.5 \times 10^{-4}$, 80 000 time-steps were required for a non-dimensional integration period of $t = 20$. For an average iteration time of around 1.53 s, the total runtime was 34 h. On the requested resources this equates to 40 800 node hours, or, equivalently, 1.96×10^6 core hours.

The first quantity is the kinetic energy, which is representative of the large-scale motion in the flow and is given as

$$E_k = \frac{1}{2\rho_0 U_0^2 |\Omega|} \int_{\Omega} \rho \mathbf{u} \cdot \mathbf{u} d\Omega. \quad (9)$$

In terms of engineering practice, this quantity is of importance as it characterizes the energy carried by the turbulent motion and is, therefore, the target quantity of interest to be captured accurately in turbulence simulations. It is carried mainly by the large vortices in the flow. At sufficiently high Reynolds numbers, the kinetic energy is conserved in the early stages of the large-scale evolution, and starts being dissipated when the turbulence cascade generates smaller scales, that are impacted by molecular viscous effects. As a result, relatively coarse grids are able to capture this quantity, as it is carried by the large scales in the flow that, depending on the accuracy of the scheme considered, require few points per vortex to be precisely described numerically. Figure 2 displays the kinetic energy evolution for a sixth-order TENO scheme and resolutions ranging from 64^3 to 2048^3 spatial degrees of freedom (DoFs). We clearly see a fast mesh convergence of this quantity, as the 128^3 resolution is sufficient to capture accurately the kinetic energy carried by large scales in the flow. Thus, this quantity will be of interest to assess the resolution needed for a given numerical scheme to capture accurately large-scale vortices. The decaying part is also relevant to evaluate how the energy transfers from large-scale into smaller-scale turbulence are handled by the scheme.

The second quantity of interest is the solenoidal part of the kinetic energy dissipation, which is directly related to the vortical motion in the flow and is given as

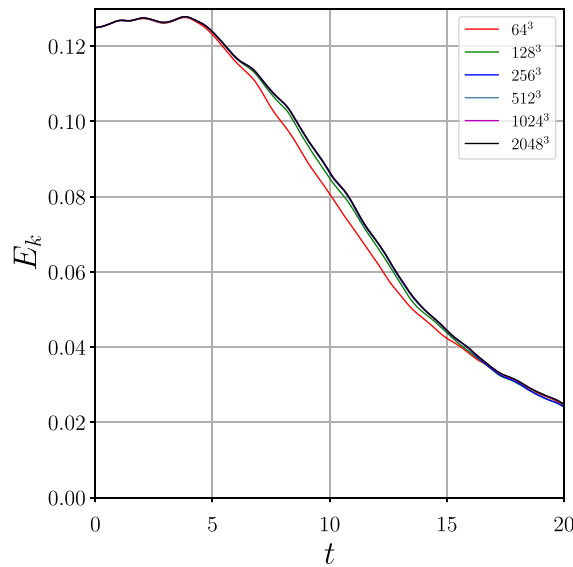


FIG. 2. Mesh convergence study for the TGV flow at $Re = 1600$ and $M_0 = 1.25$: time evolution of kinetic energy using OpenSBLI/sixth-order TENO scheme.

$$\epsilon_s = \frac{L^2}{ReU_0^2|\Omega|} \int_{\Omega} \frac{\mu(T)}{\mu_0} \omega \cdot \omega d\Omega, \quad (10)$$

where ω is the vorticity vector. This quantity is sensitive to the development of small scales in the flow, which carry a significant vortical intensity. The magnitude of this quantity increases significantly as the large-scales break into smaller structures and, therefore, provides a good diagnostic to assess the ability of a given numerical scheme to represent accurately the breakdown mechanism and small-scale structures dynamics. Compared to the kinetic energy, the solenoidal dissipation is more challenging to capture numerically, and finer resolutions/more accurate schemes are required to represent accurately this quantity. Figure 3 displays the mesh convergence for this quantity, showing here that with the sixth-order TENO scheme, a 512^3 resolution is required for converging toward the exact values and capture all turbulent scales. In this study, the amplitude of enstrophy will be directly correlated with the ability of a given numerical scheme to represent accurately small-scale turbulence.

The third quantity is the dilatational component of the kinetic energy dissipation, which is related to compressibility effects and is given as

$$\epsilon_d = \frac{4L^2}{3ReU_0^2|\Omega|} \int_{\Omega} \frac{\mu(T)}{\mu_0} (\nabla \cdot \mathbf{u})^2 d\Omega. \quad (11)$$

This quantity is strongly impacted by the onset of shocks in the flow, which are characterized by peaks in the dilatational dissipation evolution. Figure 4 displays a mesh convergence of the dilatational dissipation time evolution using the sixth-order TENO scheme. First, two peaks are clearly identified, the first being linked to shocks developing with little interaction with the vortices, while the second corresponds to the onset of shock/turbulence interaction. It is interesting to see that mesh convergence is not achieved on the first peak, as the shocks are becoming sharper corresponding to an increasing magnitude of the

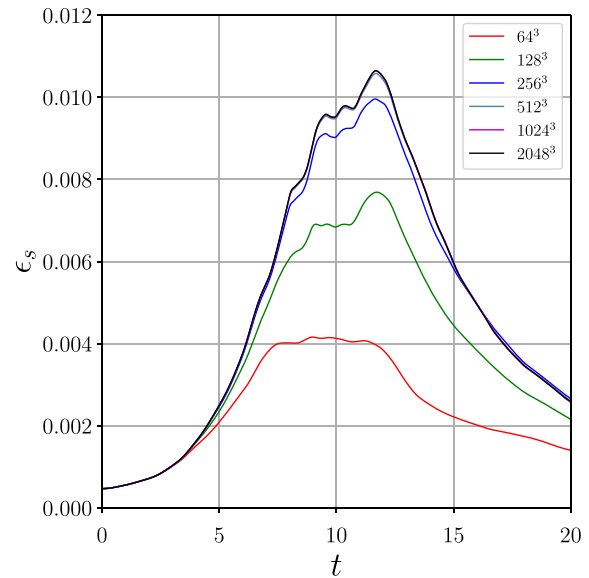


FIG. 3. Mesh convergence study for the TGV flow at $Re = 1600$ and $M_0 = 1.25$: time evolution of solenoidal dissipation using OpenSBLI/sixth-order TENO scheme.

divergence of velocity. Ultimately, a mesh convergence of velocity gradients should be reached when the molecular viscosity operator is able to smooth the shocks, which is not yet observed even with a 2048^3 resolution with 8×10^9 DoFs. The second peak seems to be mesh converging faster, possibly due to the presence of multiple shock systems, being less intense than the shocks present in the earlier flow development steps. The dilatational dissipation is, therefore, a meaningful quantity as its amplitude allows for assessing the sharpness of shocks

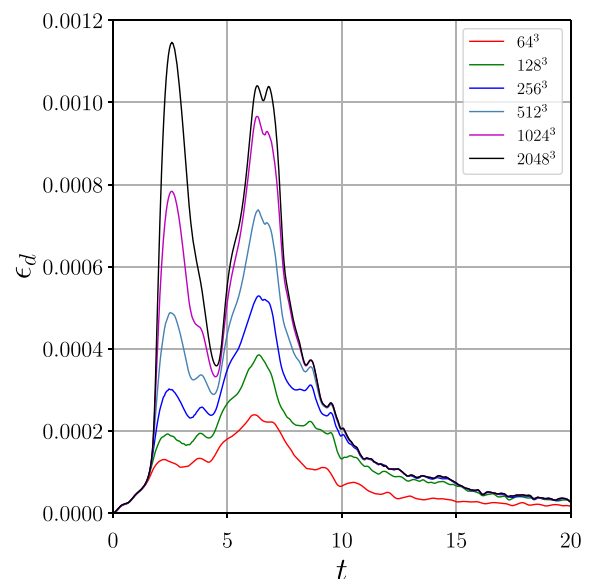


FIG. 4. Mesh convergence study for the TGV flow at $Re = 1600$ and $M_0 = 1.25$: time evolution of dilatational dissipation using OpenSBLI/sixth-order TENO scheme.

developing in the flow, and oscillations in this quantity are also a good diagnostic to detect the presence of Gibbs phenomena around the shocks, and possible flaws in the numerical strategies for shock capturing.

III. NUMERICAL METHODOLOGIES

A. Summary of numerical methodologies

This study involves different types of numerical discretization and shock capturing approaches for the simulations of the supersonic turbulent flows. Mainly two classes of solvers are considered: high-order finite difference solvers and high-order Discontinuous Finite Element solvers. In the following, a brief description of the two families is provided:

- High-Order Finite Difference approaches: FD techniques are particularly suited for turbulence simulation, as very high-orders of accuracy can be achieved on structured grids. However, shock capturing coupled with such schemes can prove difficult, as those schemes can become unstable in the presence of discontinuities. Several stabilizing techniques can be employed. The NS3D¹⁷ solver utilizes the high resolution of compact finite differences combined with high-order filtering; for this study, it was chosen to refrain from additional targeted shock-capturing approaches to stabilize the simulations. SPADE¹⁸ uses a kinetic energy/entropy preserving formulation coupled with a local switching to WENO flux reconstruction near shocks to provide stable and accurate simulations. OpenSBLI¹⁵ uses high-order TENO schemes with the shock capturing embedded in the definition of numerical fluxes while providing an accurate representation of turbulence.
- Discontinuous Finite Element approaches: the solvers SD3DvisP¹⁹ (abbreviated SD3D), CODA,²⁰ FLEXI,²¹ and H3AMR²² solve the Navier–Stokes equations using piecewise polynomial approximations of arbitrary order of accuracy per mesh element. The polynomial bases are local, meaning the continuity of the solution is not enforced at element interfaces. The elements are connected via numerical fluxes defined for the computation of interface integrals. Typically, the element sizes employed for DG or SD are larger compared to FV or FD methods due to the subcell variations of the numerical solution. This is problematic for shock capturing as a shock located inside a cell is represented by a polynomial approximation which is likely to display strong oscillations. The oscillations are controlled via a localized diffusion operator for the DG (CODA) and SD (SD3D) codes or via an embedded Finite Volume solver with a limiter (FLEXI). DG and SD methods provide accurate shock sensors, based on the amplitude of the highest polynomial modes of a given quantity (typically the density or pressure), which provide an estimation of the smoothness of the solution. SD3D features a Spectral Difference scheme, which belongs to the category of nodal DFEM, for which the DoFs are the conservative variables values at given quadrature points inside the mesh elements and the Lagrange polynomial basis is considered. CODA features a modal DG scheme for which the solution is expressed as a superposition of spatial modes, the DoFs being the magnitude of each mode (i.e., the weighting factors of the constant, linear, quadratic, or higher degree modes) and the basis functions being orthonormal and hierarchical polynomials. FLEXI features a nodal DG

scheme on a tensor product formulation of Lagrange basis functions and a collocation of interpolation and integration nodes on Legendre–Gauss-family sets.

All shock capturing approaches considered in this study, excluding the one of NS3D, rely on a specific numerical treatment around shocks, which are detected using discontinuity or smoothness sensors; therefore, it is expected that the orders of accuracy of the schemes are preserved away from discontinuities. As regards NS3D, the simulations are stabilized using a filter which order is greater than the order of accuracy of the scheme; therefore, it is expected as well to recover the nominal order of accuracy away from shocks.

As this study focuses on spatial accuracy, robustness, and shock capturing assessment, the time advance schemes considered for all flow solvers rely on classical third- or fourth-order Runge–Kutta methods, which is the standard practice for the simulation of unsteady compressible flows.⁷

In order to verify the correct implementation of the numerical set-up for each solver, computations of the Taylor–Green vortex at low Reynolds and subsonic conditions have been carried out at fine resolution and compared to ensure that all solvers provide similar solutions in the absence of shocks, see [Appendix](#). Section III B describe in more detail the flow solvers considered in the present study.

B. Flow solvers description

1. Discontinuous Galerkin solver–CODA

CODA²⁰ is the CFD software jointly owned and developed by ONERA, DLR, and Airbus with the purpose of applied research and aerodynamic design in the aeronautic industry. CODA features several numerical schemes for solving Navier–Stokes and RANS equations, including Finite Volumes and high-order Discontinuous Galerkin schemes tailored for complex geometries and mixed-element unstructured grids (featuring hexahedra, tetrahedra, pyramids, or prisms). In this work, we are interested in the DG scheme in CODA for which the numerical solution is expressed as a polynomial expansion of degree p in each of the mesh elements. The polynomial basis is constructed to verify the properties of hierarchy and orthonormality for any mesh elements.²³ The size of the basis is determined using Pascal triangle products, yielding $(p+1)(p+2)(p+3)/6$ basis functions per element in three spatial dimensions. Additional details about the formulation can be found in Ref. 24. The numerical flux chosen for the integration of the convective face fluxes is the Roe flux with an entropy fix, the entropy fraction is set to a standard value 0.1. The viscous fluxes are discretized using the BR1 approach by Bassi and Rebay,²⁵ while the time integration is performed using a third-order explicit Runge–Kutta scheme. As regards the BR1 approach, it is chosen over the BR2 approach²⁶ as it avoids tuning the penalty parameter for the BR2 gradient reconstruction on faces. The volume and face integrals appearing in the variational formulation of the DG discretization are computed using tensor-product Gauss–Legendre quadrature rules with $(p+1)^3$ and $(p+1)^2$ points, respectively. The shock capturing technique is based on the Persson and Peraire sensor²⁷ with the formulation and calibration of Glaubitz *et al.*²⁸ The idea is to identify troubled cells where shocks are present based on the amplitude of highest density polynomial modes, build an artificial viscosity scaled by the maximum wave-speed in the computational domain, and apply a localized artificial dissipation in those cells. The operator chosen for the diffusion is a

Laplacian acting on all conservative variables. To enable an accurate representation of turbulence near shocks, the artificial viscosity is multiplied on each quadrature points by the Ducros function,²⁹ which reduces its amplitude in vorticity-dominated regions. Additionally, in order to enhance robustness of the flow solver, the positivity preserving limiter of Wang *et al.*³⁰ is applied whenever a negative pressure or density is detected at an element or face quadrature point of the DG discretization.

2. Conservative finite difference solver–SPADE

Static Polymorphic Algorithms for Differential Equations (SPADE) is a newly developed library for the solution of spatially varying differential equations using finite-volume and finite-difference methods. SPADE is written in native C++20 and makes heavy use of metaprogramming to provide a device-agnostic framework for the implementation and optimization of arbitrary numerical kernels. The solver used in this study is a prototype for a new version of the CHAMPS (Cartesian High-fidelity Adaptive Multi-Physics Solver) code from University of Maryland.^{31,32}

For this study, a conservative finite-difference formulation is employed. The viscous fluxes are computed using a standard second-order scheme. To compute the inviscid fluxes, a hybrid scheme is employed as detailed in Ref. 18: two fluxes are computed, one of which is done using a centered kinetic energy and entropy preserving scheme^{33,34} (centered schemes of order 2, 4, 6, and 8 are considered in this work), and the other is a third-order upwind flux reconstruction. The two schemes are combined with a linear homotopy using the shock sensor from Ducros *et al.*²⁹ as a parameter. There is no model introduced to account for subgrid scales.

SPADE is developed jointly between the University of Oxford and the University of Maryland.

3. High-order finite difference solver–OpenSBLI

OpenSBLI¹⁵ is an open-source high-order compressible multi-block flow solver on structured curvilinear meshes, developed at the University of Southampton and JAXA. Written in Python, OpenSBLI utilizes symbolic algebra to automatically generate a complete finite-difference CFD solver in the Oxford Parallel Structured (OPS)³⁵ Domain-Specific Language (DSL). Users can define systems of partial differential equations to solve, which are expanded and discretized symbolically to create a simulation code tailored to the problem specified. The OPS library is embedded in C/C++ code, enabling massively parallel execution of the code on a variety of high-performance-computing architectures via source-to-source translation, including GPUs. OpenSBLI is explicit in both space and time, with a range of different discretization options available to users.

For smooth flows, spatial discretization is performed by arbitrary order central differences written in quadratic and cubic split forms.³⁶ Central schemes are also used for computing diffusive and heat flux terms. Shock-capturing is performed via Weighted Essentially Non-Oscillatory (WENO) and Targeted Essentially Non-Oscillatory (TENO) schemes⁸ of arbitrary order. The shock-capturing schemes can either be used to solve the convective terms directly, or, as a filter step to stabilize the non-dissipative central schemes. The shock-capturing schemes use a Local Lax–Friedrich (LLF) method to build the flux reconstruction. Time-advancement is performed by third-

fourth-order low-storage Runge–Kutta schemes.³⁷ The efficacy of the shock-capturing schemes in OpenSBLI was assessed for the compressible Taylor–Green vortex case in Ref. 6 and for compressible wall-bounded turbulence in Ref. 38. OpenSBLI also contains adaptive-TENO schemes, which further lower numerical dissipation via tuning with the addition of a shock sensor. For simplicity, however, the original sixth-order standard TENO formulation⁸ is used in this work. A TENO cutoff threshold value of $CT = 1 \times 10^{-6}$ is used here for a good balance between low numerical dissipation and robust shock-capturing.

4. High-order finite difference solver–NS3D

NS3D is a compressible high-order DNS code being continuously developed at the IAG of the University of Stuttgart. NS3D is written in FORTRAN 2008 and solves the three-dimensional, unsteady, compressible Navier–Stokes equations in conservative formulation and Laplace formulation of the viscous terms. NS3D features fully three-dimensional domain decomposition;¹⁷ communication along the internal boundaries of the resulting blocks is handled by MPI routines; in addition, the code is hybrid parallelized by means of OpenMP directives. For spatial discretization, multiple high-order finite-difference approaches are implemented; for all present computations, subdomain tridiagonal sixth-order compact finite differences are used employing several ghost derivatives outside the subdomain ends, see Refs. 39 and 40. Time advancement is performed by the classical explicit fourth-order Runge–Kutta scheme, which can be coupled with unconditionally alternating forward- and backward-biased finite differences for the convective terms, see Refs. 14 and 39. In addition, a compact tenth-order filter is used every full time step to stabilize the simulation⁴¹ (filter equal in all spatial directions, $\alpha = 0.4$), further allowing to treat the convective terms with purely central schemes for all present cases. For all NS3D simulations of the Taylor–Green test case presented in the following, stable results were already obtained without the additional use of shock capturing. Therefore, as a valuable comparison reference for cases with active shock-capturing, it was decided to calculate all NS3D results without additional shock-capturing. Obviously, however, this approach only gives high-quality results for cases with adequate DNS resolution but leads to strong oscillations in, e.g., the later shown Mach number profiles in the shock regions for the under-resolved cases. In non-dimensionalized units, the time steps for the four simulations have been chosen to be $\Delta t = 0.00125$, 0.0025, 0.005, and 0.01 for the 512^3 , 256^3 , 128^3 , and 64^3 resolution cases, respectively. Post-processing is performed with sixth-order compact finite differences and, thus, with the same schemes as the simulations were run. For lower orders, e.g., explicit fourth-order finite differences, deviations in ϵ_s of up to 5% have been found for the supersonic case.

5. High-order spectral difference solver–SD3DvisP

The SD3DvisP solver, originally developed by Antony Jameson's group at Stanford University, is an MPI parallelized FORTRAN 90 code for compressible viscous flows based on the high-order spectral difference (SD) scheme for unstructured hexahedral elements.^{10,19,42,43} Inviscid numerical fluxes at element interfaces are computed via the Roe's Riemann solver with entropy fix.⁴⁴ In particular, the first Harten and Hyman entropy correction is considered.^{45,46} As regards the viscous fluxes, the centered flux introduced by Sun *et al.*⁴² is considered.

The time integration is done explicitly with a third-order, three-stage, total variation diminishing (RK33-TVD) Runge–Kutta scheme.⁴⁷ The shock capturing technique considered for SD3DvisP is described in detail in Lodato⁴⁸ and is based on the sub-cell shock capturing method^{27,49} with the shock sensor based on density modes and the artificial viscosity parameters (including the ramp and threshold parameters) being set using a self-calibration procedure. The amplitude of artificial viscosity C_v is set to 0.5 instead of 1 to avoid too strong CFL restrictions. The artificial viscosity is first computed as a single value in each mesh element, then made C_0 continuous via linear interpolation. To do so, an average of the artificial viscosity values is computed at each node of the mesh from the values in the surrounding elements, then local linear interpolations weights are found using the eight nodal values per hexahedral element corresponding to the elements vertices. The artificial viscosity values are then interpolated at volume quadrature points. The artificial diffusion operator considered is the one presented in Tonicello *et al.*,⁵⁰ where the artificial diffusion acts as a bulk viscosity on the momentum equations, and as a thermal diffusivity on the energy equation. No artificial diffusion is considered for the mass conservation equation. A positivity preserving procedure is also employed to enhance the robustness of the simulations.^{48,51}

6. Discontinuous Galerkin spectral element solver–FLEXI

FLEXI⁵² is an open source framework for solving hyperbolic–parabolic systems of equations on unstructured grids via a high-order Discontinuous Galerkin Spectral Element Method (DGSEM).²¹ The main areas of application of FLEXI are multiscale/multiphase/multi-physics problems of compressible aerodynamics.⁵³ FLEXI is developed and maintained by the Numerics Research Group at the IAG of the University of Stuttgart. The framework consists of the open source high-order preprocessor HOPR⁵⁴ for handling and generation of curved, unstructured grids, the PDE solver FLEXI and a high-order postprocessing suite with ParaView plugin. All parts are written in FORTRAN 2008 and parallelized with MPI3.0; strong scaling on up to 262,000 CPUs shows superlinear behavior down to one element per processor.⁵⁵

In this study, FLEXI discretizes the compressible Navier–Stokes equations by a fourth-order accurate DGSEM scheme in space, optionally combined with a subcell Finite Volume method to capture regions with shocks. Temporal integration is performed by a fourth-order accurate low storage, explicit Runge–Kutta scheme.³⁷ In the DGSEM formulation, the solution is approximated by tensor products of 1D-Lagrange polynomials of arbitrary degree N on a reference element. The local polynomial degree can be adapted dynamically to the solution. The nodes for this basis are chosen as Legendre–Gauss or Legendre–Gauss–Lobatto points. This collocation of interpolation and integration points transfers the tensor product structure to the DG operator and results in dimension-by-dimension operations, as opposed to volume operations in other DG variants. As an inviscid numerical flux function, the approximate Riemann solver by Roe with an entropy fix is used. The second entropy fix of Harten and Hyman was used,⁴⁶ which has the benefit of not having a user-defined constant entropy-fix threshold. For the viscous fluxes, the first method of Bassi and Rebay is chosen.²⁵ Various subgrid scale closure models for LES computations are available; however, in this study, no explicit modeling of the unclosed terms is present. Shock capturing is based on a

hybrid Finite Volume/DGSEM scheme. In grid elements in which a suitable sensor detects the occurrence of a shock wave, the DG solution is projected onto a compatible FV subgrid (Cartesian in reference space) that shares the same data-structure as the DG solution. On this element-local subgrid, instead of the DGSEM scheme, a second-order TVD FV scheme with a generalized minmod limiter⁵⁶ is solved. To detect discontinuous solution features, an indicator based on the modal decomposition of the polynomial solution ansatz is employed. It is evaluated on the pressure and infers the smoothness of the element local solution from the exponential decay rate of the modes.^{57,58} The combination of a high-order DG scheme with a local and robust FV formulation allows an efficient resolution of smooth regions and a sharp capturing of discontinuities through an adaptation of the approximation space to the underlying solution. More details on this hybrid DGSEM/FV scheme, its implementation, and validation for single- and multiphase flows can be found in Refs. 57, 59, and 60.

7. Flux Reconstruction solver–H3AMR

H3AMR (HySonic, High-Order, Hybrid Adaptive Mesh Refinement)^{22,61,62} is an in-house code developed by HySonic Technology, LLC. The code solves the compressible Navier–Stokes equations using the flux reconstruction¹² numerical scheme for unstructured meshes. The solver is based on block-spectral,¹⁰ and therefore, the simulation domain is divided into blocks—or mesh elements—and inside each element, the solution is stored at N Gauss–Legendre quadrature points in each direction, N corresponding here also to the spatial order of accuracy. Hence, the number of elements is equal to the number of DoFs divided by N^3 . The code has several capabilities from different LES and shock capturing methods to h and p refinement capabilities. For the purpose of this work, we are going to explain only the functionality used for this simulation. Time advancement is a third-order Runge–Kutta method. The flux reconstruction method relies on an average of different orders of Radau polynomials to compute the correction functions and the fluxes are updated at the faces using the Rusanov method. The shock capturing method is a new numerical method developed in Carlo Scalo's group at Purdue University called Block Spectral Stresses (BSS),⁶³ able to do shock-capturing and turbulence modeling at the same time. The modeling is specifically developed for the flux reconstruction method and it relies on the spectra of the velocity gradient to compute the sub-filter stresses, heat flux, and pressure work.

8. Summary of shock capturing approaches

In this paragraph, the various shock capturing strategies considered for the present study are briefly reviewed. All of them introduce additional numerical dissipation or limiting with the aim of smoothing the numerical solution around shocks and mitigate the Gibbs oscillations.

To do so, SD3D, CODA, and H3AMR use a dissipation operator explicitly added to the Navier–Stokes equations. For SD3D and CODA, it takes the form of a Laplacian operator impacting all conservative variables, while for H3AMR, the dissipative operator mimics a molecular dissipation, impacting the momentum and total energy variables. The strategies in FLEXI, SPADE, and OpenSBLI aim at switching locally to a lower-order scheme featuring improved shock-capturing properties. FLEXI uses a second-order FV scheme with the

total variation diminishing property, while SPADE uses a third-order weighted-essentially non-oscillatory (WENO) scheme. As regards OpenSBLI, the switch to lower-order is part of the design of the TENO method. NS3D considers a filtering of the numerical solution using a high-order finite difference operator, which effectively smoothes the solution at all time steps.

A second important ingredient common to all present methodologies, except NS3D, is the sensor driving the local activation of the specific shock-capturing treatment. The discontinuous finite element-based schemes SD3D, CODA, FLEXI, and H3AMR exploit the element-wise polynomial information to devise such sensor. SD3D and CODA use the sensor introduced by Persson and Peraire,²⁷ which isolates the highest density polynomial mode in the element, providing a local estimation of the smoothness of the numerical solution. FLEXI uses a similar idea by estimating the exponential decay of the polynomial modes magnitude in the elements.⁵⁸ H3AMR also uses the energy related to the highest polynomial mode of momentum to activate locally the shock-capturing treatment.⁶³ SPADE uses the well-known Ducros function²⁹—which tends to 0 when the vorticity magnitude locally dominates the divergence of velocity magnitude and to 1 otherwise—to blend the high-order and diffusive spatial schemes. The TENO scheme in OpenSBLI relies as well on smoothness indicators based on the polynomials used for the reconstruction of the numerical solution.

IV. SUPERSONIC TAYLOR-GREEN VORTEX SIMULATIONS: RESULTS AND DISCUSSION

A. Integrated quantities

This section presents the results obtained with the various flow solvers introduced in Sec. III for the simulation of the supersonic Taylor–Green vortex at Mach 1.25 and Reynolds number 1600. A summary of the solvers, numerical methods, order of accuracy, and type of shock capturing is displayed in Table I. All solvers are considering high orders of accuracy except for H3AMR which runs with a second order of accuracy. This is of interest to assess how high-order schemes behave compared to standard second-order schemes for such problems. A mesh convergence study is performed considering four resolution levels with respectively 64^3 , 128^3 , 256^3 , and 512^3 degrees of freedom. Regarding finite difference-based solvers, the number of DoFs is equivalent to the number of mesh points considered. However, for discontinuous finite element solvers, considering the polynomial resolution inside elements, the total number of DoFs is higher than the number of mesh elements, and summarized in Table II. The 64^3 DoFs resolution is coarse

TABLE I. Summary of numerical methods employed in the present study.

Solver	Numerical method	Order of accuracy	Shock capturing
CODA ²⁰	Modal DG	4	LAD
SPADE ¹⁸	Central FD	8	Local upwinding
OpenSBLI ¹⁵	FD-TENO	6	TENO
NS3D ¹⁷	Central FD	6	HO filter
SD3DvisP ¹⁹	SD	4	LAD
FLEXI ²¹	DGSEM	4	Subgrid FV
H3AMR ²²	FR	2	LAD

TABLE II. Number of mesh elements and DoFs for discontinuous finite element discretization.

Solver	Order of accuracy	No. of mesh elements	No. of DoFs
CODA ²⁰	4	$23^3-47^3-94^3-189^3$	243 340–2 076 460–16 611 680–135 025 380
SD3DvisP ¹⁹	4	$16^3-32^3-64^3-128^3$	$64^3-128^3-256^3-512^3$
FLEXI ²¹	4	$16^3-32^3-64^3-128^3$	$64^3-128^3-256^3-512^3$
H3AMR ²²	2	$32^3-64^3-128^3-256^3$	$64^3-128^3-256^3-512^3$

and is not expected to fully resolve the fine turbulent scales or the shock features. This coarse resolution might be relevant for large-eddy simulation modeling; however, considering the relatively low Reynolds number of this configuration, we assume in this work that the inherent dissipative properties of the considered numerical schemes are sufficient to mimic the subgrid dissipation. For the 512^3 DoFs resolution, we expect the turbulent scales to be fully or nearly fully resolved, while the shock profiles are expected to become sharper but not fully resolved.

Figures 5–7 display the time evolution of kinetic energy, dilatational dissipation, and solenoidal dissipation, respectively. The results are presented for all solvers and resolutions.

Regarding the kinetic energy evolution, all solvers are able to capture it accurately with 128^3 DoFs and above. Although the agreement is also good for the 64^3 grid, this resolution features the most differences between flow solvers and is, therefore, interesting to discuss further. An underestimation of kinetic energy levels in the early stages is observed for the CODA (DG), SD3DvisP (SD), and OpenSBLI (TENO) flow solvers. This behavior is likely to be related to the intrinsic numerical dissipation of these schemes, stemming from Riemann-based numerical fluxes defined at the interfaces between elements. On the other hand, the SPADE and NS3D solvers based on numerical dissipation-free high-order FD strategies provide a very accurate prediction of kinetic energy on the coarse grid in the early and intermediate flow regimes (about up to $t = 12$), but display slightly excessive levels in the later stages ($t > 12$), for which the turbulence is fully developed and the large-scale energy cascade communicates kinetic energy toward the smallest scales that can be represented by the discretization. This behavior could be explained by a slight small-scale energy pileup located around the grid cutoff wavenumber and a lack of subgrid scale closure, as in this case the central FD schemes (unlike upwinded schemes) do not introduce a sufficient numerical dissipation that could mimic the subgrid dissipation. The results of FLEXI are more consistent with the FD-based solvers SPADE and NS3D, despite using the same Riemann-based flux approximations as CODA and SD3DvisP. However, the shock capturing strategy of FLEXI, and thus, the introduced numerical diffusion differs considerably from the LAD approaches, which likely explains these differences. Finally, the H3AMR second-order 64^3 DoFs simulation displays underestimated kinetic energy levels representative of an excess of numerical dissipation, typically found for second-order upwind schemes. It is interesting to verify that higher-order schemes with the same number of DoFs have better kinetic energy resolution properties in this case. Overall, the present results confirm that all schemes considered provide an accurate representation of the large turbulent scales in the flow, and

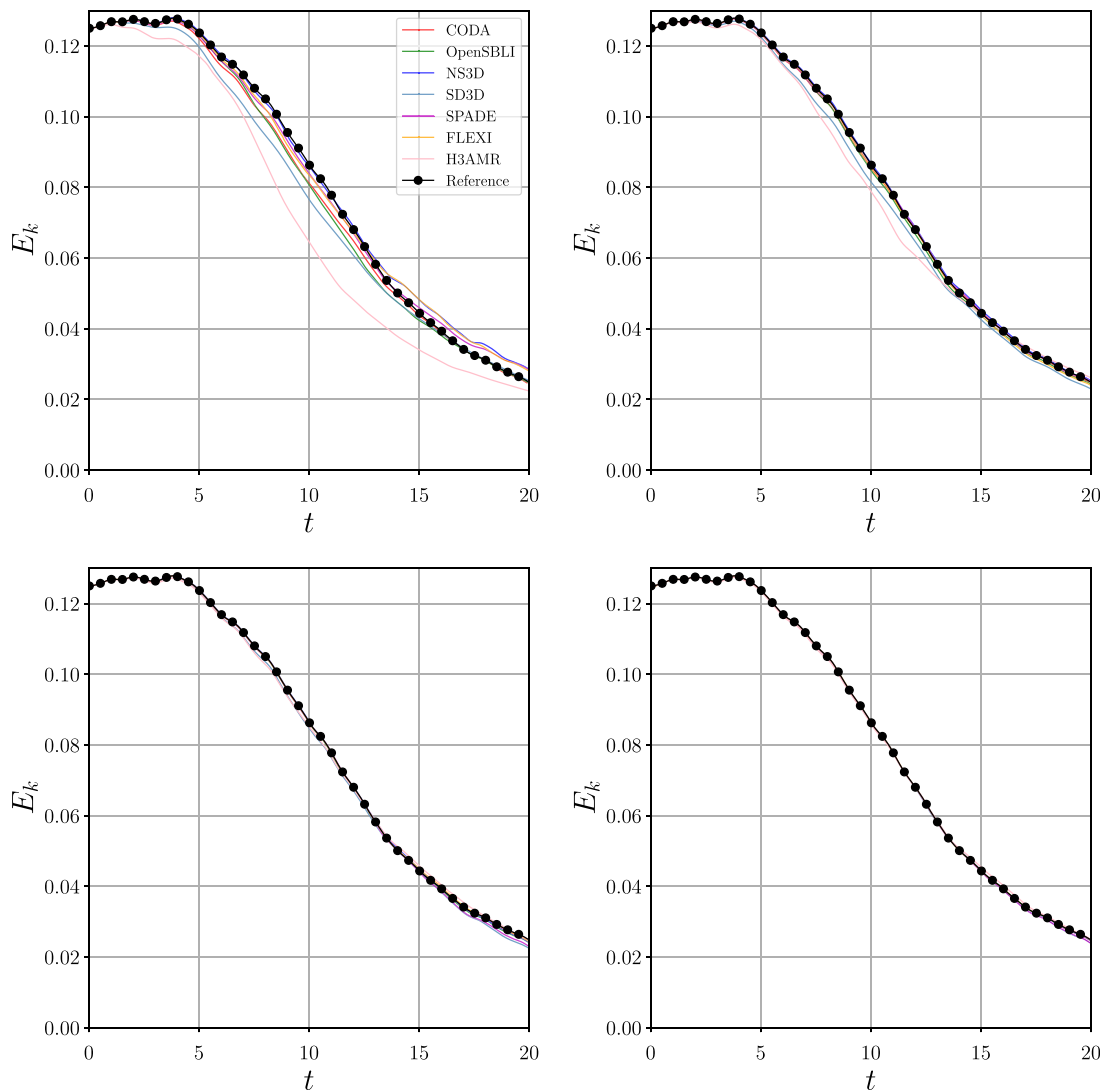


FIG. 5. Code comparison study for the TGV flow at $Re = 1600$ and $M_0 = 1.25$: time evolution of kinetic energy for the four resolutions considered. Top left: 64^3 DoFs; top right: 128^3 DoFs; bottom left: 256^3 DoFs; bottom right: 512^3 DoFs. Reference: 2048^3 sixth-order TENO simulation.

therefore, low numerical dissipation levels in the lower wavenumber range, which is a typical feature of high-order schemes that all solvers manage to preserve in this compressible/shock–turbulence interaction case.

The dilatational dissipation levels, governed by the magnitude of divergence of velocity, are mainly driven by strong compression and dilatation effects, which in turn leads to a significant contribution of shocks that are numerically correlated with important divergence levels. Low levels of dilatational dissipation will tend to indicate that a given shock capturing method is strong, and yield smooth and thick shock profiles. Conversely, methods able to yield sharp shock profiles will display higher levels, with the risk of producing oscillations that can also appear in the time evolution of dilatational dissipation. We can clearly see that NS3D, which features a high-order central FD

scheme coupled with a high-order filtering, yielding overall low levels of shock-dissipation, produces the highest magnitude of dilatational dissipation among the solvers considered, with oscillations around the first peak identified for all resolutions. FLEXI results display a slightly lower dissipation and comparable oscillations for the lower resolutions. This behavior is due to the switching of the DG operator to a FV operator and back for individual grid elements as shock appear or decay. Next, CODA (DG) and OpenSBLI (TENO) provide lower levels, but with reduced oscillations, in particular for OpenSBLI which is clear of oscillations regardless of the grid resolution. CODA starts displaying slight oscillations around the first peak with the 256^3 resolution, which could be related to the locality of artificial diffusivity, which transitions sharply from zero to maximal values in cells where shocks are localized. SPADE, SD3D, and H3AMR appear to be the most impacting

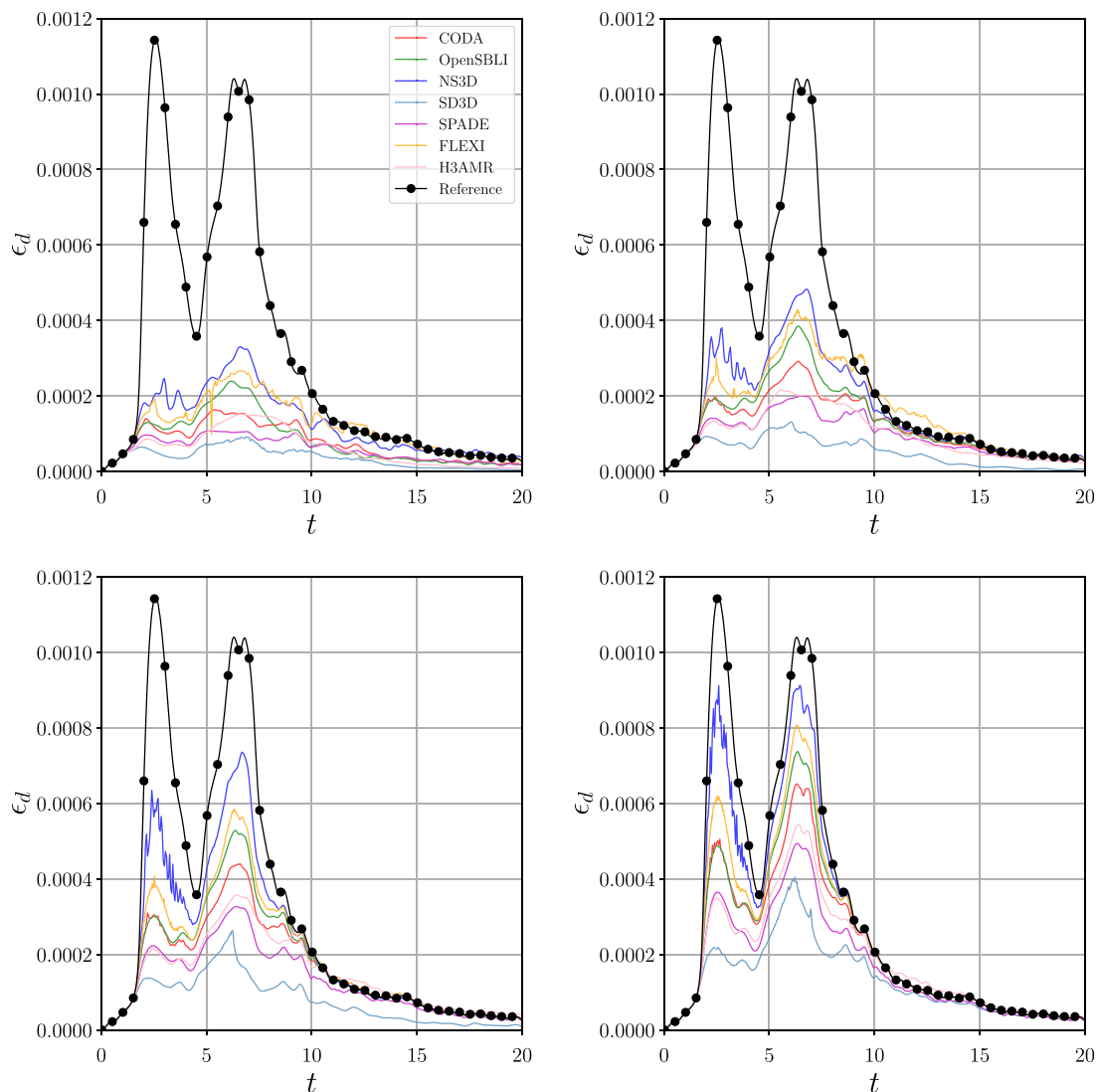


FIG. 6. Code comparison study for the TGV flow at $Re = 1600$ and $M_0 = 1.25$: time evolution of dilatational dissipation for the four resolutions considered. Top left: 64^3 DoFs; top right: 128^3 DoFs; bottom left: 256^3 DoFs; bottom right: 512^3 DoFs. Reference: 2048^3 sixth-order TENO simulation.

solvers with respect to shock capturing and display the lower levels of dilatational dissipation on all grids.

Finally, the solenoidal dissipation, being correlated with the quality of resolution of the smaller turbulent scales, is assessed. This quantity is more challenging to capture correctly compared to the kinetic energy as seen from Fig. 7 and is also likely to be impacted by the shock capturing strategy, which might dissipate excessively small turbulent scales. Some discrepancies are observed between flow solvers, in particular considering the coarser resolutions. The rate of convergence with respect to the resolution also differs from method to method. CODA, FLEXI, and NS3D display the highest levels on all grids, which could be explained by their relatively lenient shock capturing approach, that does not interfere much with the onset and dynamics of the small turbulent scales. It is interesting to note that NS3D provides smooth solenoidal dissipation evolutions, as well as satisfactory mesh convergence, which indicates that a mild shock

capturing approach does not seem to impact the characterization of small vortices. SPADE displays lower levels, which in the same fashion can be explained by the interaction of the shock capturing scheme with the development of small vortices. SD3D starts off with high levels of solenoidal dissipation on the coarse grid, but falls in the lower range for more refined resolutions. Here again, its strong shock capturing strategy is probably hindering to some extent the development of small scales on the finer grids. Finally, OpenSBLI displays low levels on coarse grids but good convergence properties, as its levels of solenoidal dissipation move into the higher range among flow solvers when the grid is refined. As regards the H3AMR results, they clearly show that second-order schemes struggle with capturing accurately fine turbulent scales, as the levels are lower compared to higher-order solvers for all resolutions. Here again, the interest of increasing the order of accuracy for an accurate capture of shocks interacting with small-scale turbulence is emphasized.

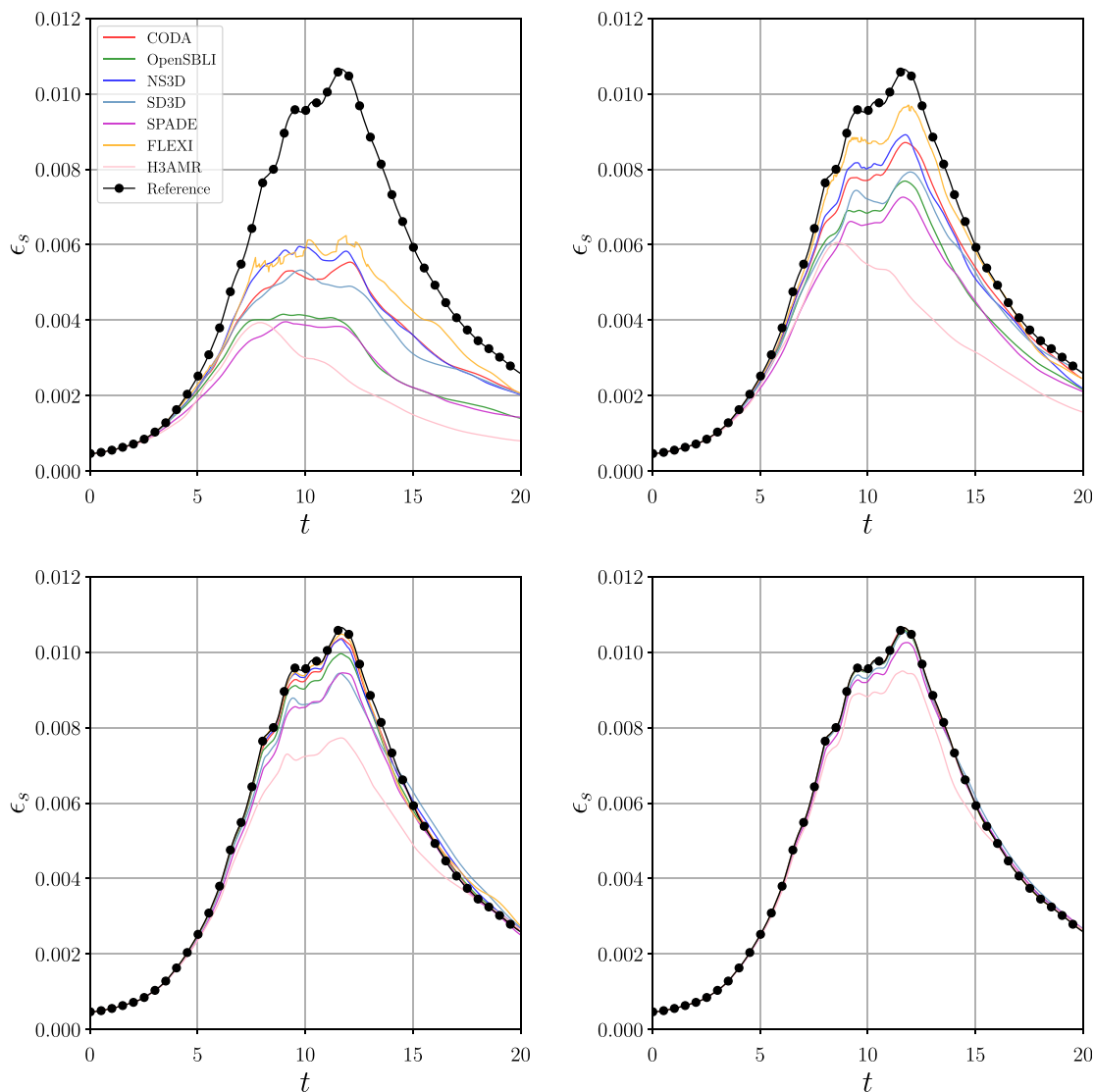


FIG. 7. Code comparison study for the TGV flow at $Re = 1600$ and $M_0 = 1.25$: Time evolution of solenoidal dissipation for the four resolutions considered. Top left: 64^3 DoFs; Top right: 128^3 DoFs; bottom left: 256^3 DoFs; bottom right: 512^3 DoFs. Reference: 2048^3 sixth-order TENO simulation.

Overall, all solvers display a comparable and consistent behavior regarding the solenoidal dissipation, showing that most of the turbulent dynamics is captured by all solvers using a resolution of 256^3 DoFs or above. For coarser grids, present results emphasize that high-order schemes are still able to capture a significant part of the small-scale dynamics. In particular, discontinuous finite elements schemes seem to be efficient in that respect. For all high-order schemes, the solenoidal dissipation plots show that small turbulent scales are better represented with respect to a second-order discretization.

B. Mach profiles

In this part, the numerical representation of shocks by the various methods is assessed from Mach profiles extracted along $x = z = 0$ y

lines in the computational domain. The chosen time is $t = 2.5$, which corresponds to the peak of dilatational dissipation, for which the shocks are the strongest.

The results are displayed in Fig. 8 for the four resolutions considered. We can observe different behavior between the various flow solvers. On the coarser grids featuring 64^3 and 128^3 DoFs, NS3D, which only relies on a high-order filter for stabilization without any particular treatment of shocks, clearly displays the strongest Gibbs oscillations. On the other hand, SD3D, which features the strongest shock capturing approach, displays oscillation-free but thick shock representations. The TENO6 scheme of OpenSBLI displays sharp shocks and is oscillation-free for all cases considered. CODA also displays sharp profiles with limited oscillations on all grids, emphasizing the potential of Discontinuous Galerkin type of discretization to capture shocks

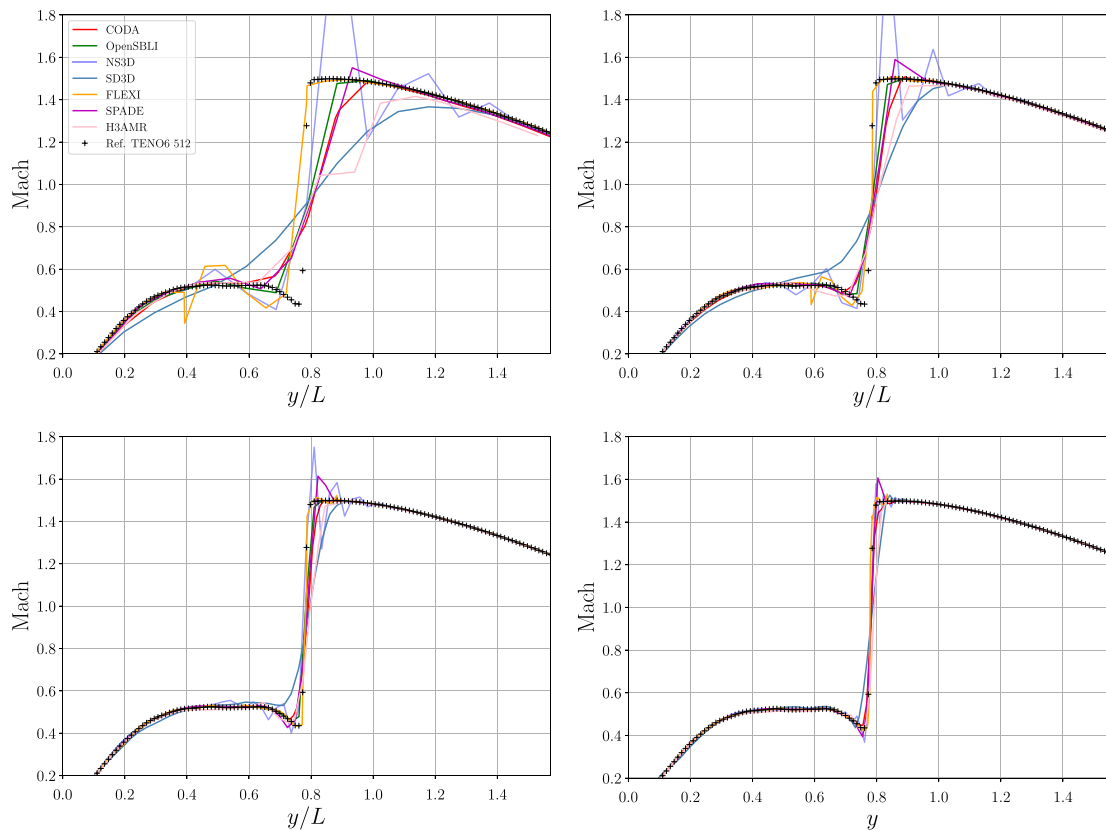


FIG. 8. Code comparison study for the TGV flow at $Re = 1600$ and $M_0 = 1.25$: Mach profiles extracted from the y line at $x = z = 0$, for the four resolutions considered. Top left: 64^3 DoFs; top right: 128^3 DoFs; bottom left: 256^3 DoFs; bottom right: 512^3 DoFs.

efficiently despite the large element sizes. The shock profiles produced by FLEXI are the sharpest ones due to the embedded FV scheme. They match the reference solution shock profiles on the 256^3 grid, but show oscillations below this resolution. In summary, while all presented solvers converge toward the reference solution, this comparison stresses the consequences of different numerical strategies and highlights the complex, non-linear interplay between discretization properties, shock capturing, and turbulent flows. In particular, this study shows the difficulty of obtaining a consistent shock capturing technique across all resolutions considered. Indeed, several shock capturing techniques are found to produce oscillations on coarse grids, which vanish when the mesh is refined. TENO schemes and LAD-based schemes seem to perform better at mitigating shock oscillations for all grid resolutions. This topic could be investigated in future research to yield further improvements of the proposed techniques.

V. CONCLUSIONS

Several high-order spatial schemes were tested for the shock–turbulence interaction problem stemming from the supersonic Taylor–Green case at Reynolds 1600 and Mach 1.25. The spatial discretization approaches featured both high-order finite element and high-order finite differences with a variety of shock capturing techniques including LAD, filtering, upwind numerical fluxes, and subcell limiting. From the time evolution of kinetic energy, integrated over the

computational domain, the large-scale dynamics were found to be accurately captured by all high-order schemes, even considering coarse grids. Solenoidal dissipation plots also showed an accurate representation and fast mesh convergence regarding the small-scale dynamics. Mach profiles and dilatational dissipation plots showed differences in the treatment of shocks by the various numerical strategies considered. Strong shock capturing strategies yield thick shock profiles and low levels of dilatational dissipation, while more lenient strategies tend to display Gibbs oscillations and high levels of dilatational dissipation.

Overall, this study showed the capability of high-order schemes to represent accurately turbulence dynamics in a compressible setting, with a low impact of the shock capturing treatment on the representation of turbulent scales. A few notable points can be highlighted:

- In terms of shock capturing methods, all approaches considered were able to provide a qualitatively similar representation of shocks on fine grids. Most differences were observed on coarser grids, for which it was found that approaches combining artificial diffusion yield smooth but thick shock profiles, while approaches relying on local switching to lower-order schemes tend to provide sharp but oscillating shocks, except the TENO scheme that displays relatively sharp shocks without oscillations. The finite difference scheme using only a high-order filter to stabilize simulations provided the highest oscillations.

- In terms of spatial accuracy, all high-order schemes considered provided an accurate representation of the kinetic energy and large turbulent scales, even considering coarser grids. As regards solenoidal dissipation and small-scale dynamics, solvers provided similar results on fine grids but differences were observed on the coarser grids. Discontinuous finite element schemes—including DG, SD, and DGSEM variants—captured well the small scales on coarser grids as well as high-order finite difference with high-order filtering stabilization. Finite difference with local scheme switching as well as high-order TENO yield more small-scale dissipation. Overall, better large- and small-scale turbulence resolution properties were found for high-order schemes against second-order solutions, even in the present challenging compressible setting.
- The dilatational dissipation quantity provides valuable information on the representation of shocks by the numerical method. Its amplitude is directly related to the strength of the shock capturing method and the shock thickness. Strong LAD-based shock capturing techniques, such as the one used in the SD3D code, yield the lowest values and thicker shock profiles while NS3D, which features only a stabilization technique with no specific shock treatment, yields the highest values and strong shock oscillations. Oscillations in time of the dilatational dissipation were also found to be correlated with Gibbs oscillations around shocks. In future studies, additional quantities characterizing compressibility effects could be considered—such as the temperature variance⁷—in order to quantify better the quality of resolution of such effects by the numerical methods.

This study has highlighted some methodological aspects that could benefit from future improvements: reduce shock oscillations for approaches based on a local switch to a lower-order scheme; increase shock sharpness while keeping low oscillations for artificial viscosity-based approaches; and pursue the development of shock or smoothness sensor to maximize the quality of both shock and turbulence resolution for any grid refinement.

This study focused on the assessment of spatial discretization schemes, but future investigation could also address the assessment of time integration schemes and their influence on the accuracy and performance of simulations.

The current work showed promising progress in the development of a variety of high-order schemes—including FD, SD, DG, DGSEM, and FR—in order to perform accurate and robust numerical simulations of complex phenomena involving strong shocks and turbulence. Applications of interest involve cruising aircraft configurations, atmospheric re-entry vehicles, supersonic engines, or astrophysical fluid dynamics.

Future research will consider similar comparison of numerical approaches for more complex cases, including shocks interacting with wall-bounded turbulence.

AUTHOR DECLARATIONS

Conflict of Interest

The authors have no conflicts to disclose.

Author Contributions

Jean-Baptiste Chapelier: Conceptualization (equal); Investigation (lead); Methodology (equal); Writing – original draft (lead). **David J. Lusher:** Conceptualization (equal); Investigation (equal); Methodology (equal); Writing – review & editing (equal). **Willam Van Noordt:**

Conceptualization (equal); Investigation (equal); Methodology (equal); Writing – review & editing (equal). **Christoph Wenzel:** Conceptualization (equal); Investigation (equal); Methodology (equal); Writing – review & editing (equal). **Tobias Gibis:** Conceptualization (equal); Investigation (equal); Methodology (equal); Writing – review & editing (equal). **Pascal Mossier:** Conceptualization (equal); Investigation (equal); Methodology (equal); Writing – review & editing (equal). **Andrea Beck:** Conceptualization (equal); Investigation (equal); Methodology (equal); Writing – review & editing (equal). **Guido Lodato:** Conceptualization (equal); Investigation (equal); Methodology (equal); Writing – review & editing (equal). **Christoph Brehm:** Conceptualization (equal); Investigation (equal); Methodology (equal); Writing – review & editing (equal). **Matteo Ruggeri:** Conceptualization (equal); Investigation (equal); Methodology (equal); Writing – review & editing (equal). **Carlo Scalo:** Conceptualization (equal); Investigation (equal); Methodology (equal); Writing – review & editing (equal). **Neil Sandham:** Conceptualization (equal); Investigation (equal); Methodology (equal); Writing – review & editing (equal).

DATA AVAILABILITY

The data that support the findings of this study are available from the corresponding author upon reasonable request.

APPENDIX: CODE VERIFICATION, TGV CASE AT $Re = 500$, $M_0 = 0.5$

This Appendix presents a verification study of the flow solver implementations of the Taylor–Green vortex case, including the various codes considered in the present study. To alleviate the computational burden of this verification and the potential variations due to shock capturing techniques, the flow conditions are set to

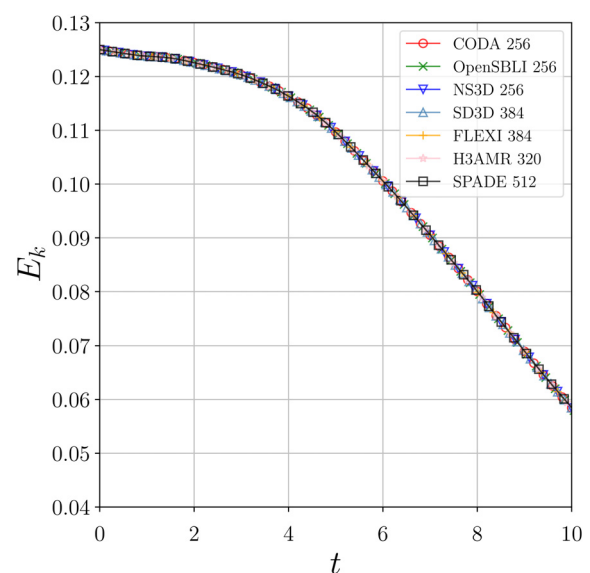


FIG. 9. Code validation for the TGV flow at $Re = 500$ and $M_0 = 0.5$: time evolution of kinetic energy.

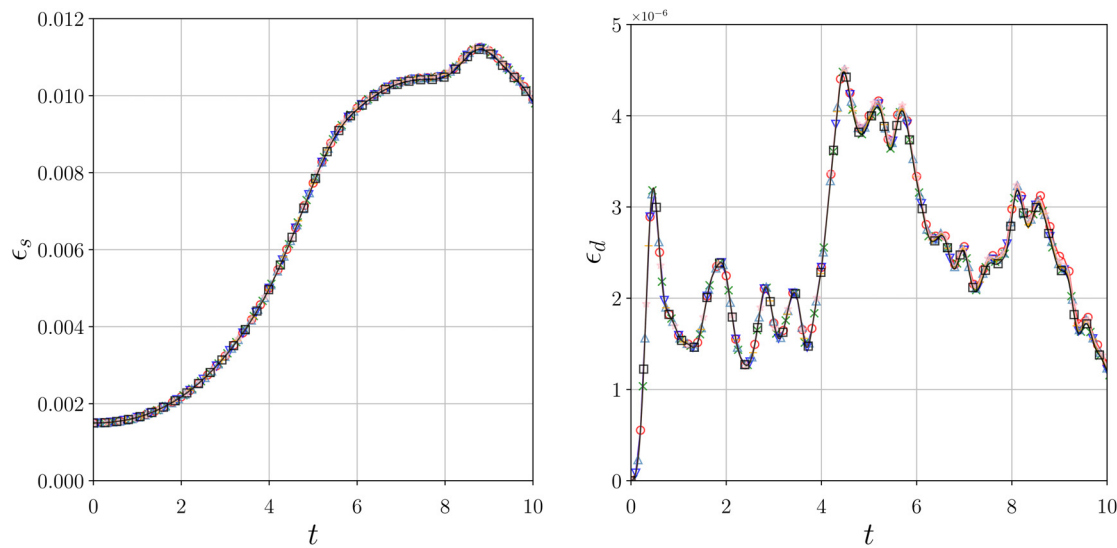


FIG. 10. Code validation for the TGV flow at $Re = 500$ and $M_0 = 0.5$: time evolution of solenoidal dissipation (left) and dilatational dissipation (right).

$Re = 500$ and $M_0 = 0.5$, ensuring a limited turbulent scales development and a subsonic regime. The target resolution is 256^3 DoFs, which should suffice for most numerical schemes, based on the observation that a case at $Re = 500$ and $M_0 = 0.1$ was fully resolved in terms of kinetic energy and enstrophy using a Fourier spectral method and 128^3 DoFs.⁵ For the present simulations, minor offsets were observed for the SPADE and SD3D codes using a 256^3 resolution; hence, 512^3 and 384^3 resolution were considered for these codes, respectively, to ensure that the offsets were due to insufficient mesh convergence rather than problems in the initialization and discretization. As regards H3AMR, a 320^3 DoFs resolution with a fourth-order of accuracy was considered for this verification run. The simulations are run up to $t = 10$, which is sufficient to assess the code behavior from the initial condition to the end of the turbulent small-scales build-up process. The results of the verification runs are shown in Figs. 9 and 10. We find that the agreement between codes is perfect for the time evolution of kinetic energy and solenoidal dissipation, showing an identical representation of the full extent of turbulent scales by all codes and methods. The same observation applies for the dilatational dissipation up to $t = 9$, after which there are minor discrepancies between codes, probably due to high resolution needed for capturing short acoustic waves radiated by the small-scale turbulent structures. Overall, the verification test is successful in confirming that all codes provide a sound implementation of the compressible Taylor–Green vortex case considered in the present study.

REFERENCES

- M. E. Brachet, D. I. Meiron, S. A. Orszag, B. Nickel, R. H. Morf, and U. Frisch, "Small-scale structure of the Taylor–Green vortex," *J. Fluid Mech.* **130**, 411–452 (1983).
- Z. J. Wang, K. Fidkowski, R. Abgrall, F. Bassi, D. Caraeni, A. Cary, H. Deconinck, R. Hartmann, K. Hillewaert, H. T. Huynh *et al.*, "High-order CFD methods: Current status and perspective," *Int. J. Numer. Methods Fluids* **72**, 811–845 (2013).
- C. Carton de Wiart, K. Hillewaert, M. Duponcheel, and G. Winckelmans, "Assessment of a discontinuous Galerkin method for the simulation of vortical flows at high Reynolds number," *Int. J. Numer. Methods Fluids* **74**, 469–493 (2014).
- G. J. Gassner and A. D. Beck, "On the accuracy of high-order discretizations for underresolved turbulence simulations," *Theor. Comput. Fluid Dyn.* **27**, 221–237 (2013).
- J.-B. Chapelier, M. De La Llave Plata, F. Renac, and E. Lamballais, "Evaluation of a high-order discontinuous Galerkin method for the DNS of turbulent flows," *Comput. Fluids* **95**, 210–226 (2014).
- D. J. Lusher and N. D. Sandham, "Assessment of low-dissipative shock-capturing schemes for the compressible Taylor–Green vortex," *AIAA J.* **59**, 533–545 (2021).
- E. Johnsen, J. Larsson, A. V. Bhagatwala, W. H. Cabot, P. Moin, B. J. Olson, P. S. Rawat, S. K. Shankar, B. Sjögren, H. C. Yee *et al.*, "Assessment of high-resolution methods for numerical simulations of compressible turbulence with shock waves," *J. Comput. Phys.* **229**, 1213–1237 (2010).
- L. Fu, X. Y. Hu, and N. A. Adams, "A family of high-order targeted ENO schemes for compressible-fluid simulations," *J. Comput. Phys.* **305**, 333–359 (2016).
- B. Cockburn, "Discontinuous Galerkin methods for convection-dominated problems," in *High-Order Methods for Computational Physics* (Springer, 1999), pp. 69–224.
- D. A. Kopriva and J. H. Kolas, "A conservative staggered-grid Chebyshev multidomain method for compressible flows," *J. Comput. Phys.* **125**, 244–261 (1996).
- Y. Liu, M. Vinokur, and Z. J. Wang, "Spectral difference method for unstructured grids I: Basic formulation," *J. Comput. Phys.* **216**, 780–801 (2006).
- H. T. Huynh, "A flux reconstruction approach to high-order schemes including discontinuous Galerkin methods," AIAA Paper No. AIAA 2007-4079, 2007.
- S. K. Lele, "Compact finite difference schemes with spectral-like resolution," *J. Comput. Phys.* **103**, 16–42 (1992).
- M. J. Kloker, "A robust high-resolution split-type compact FD scheme for spatial direct numerical simulation of boundary-layer transition," *Appl. Sci. Res.* **59**, 353 (1997).
- D. J. Lusher, S. P. Jammy, and N. D. Sandham, "OpenSBLI: Automated code-generation for heterogeneous computing architectures applied to compressible fluid dynamics on structured grids," *Comput. Phys. Commun.* **267**, 108063 (2021).
- L. Fu, "Review of the high-order TENO schemes for compressible gas dynamics and turbulence," *Arch. Computat. Methods Eng.* **30**, 2493–2526 (2023).

- ¹⁷C. Wenzel, J. M. F. Peter, B. Selent, M. Weinschenk, U. Rist, and M. J. Kloker, "DNS of compressible turbulent boundary layers with adverse pressure gradients," in *High Performance Computing in Science and Engineering*, edited by W. E. Nagel (Springer, 2018).
- ¹⁸W. van Noordt, S. Ganju, and C. Brehm, "An immersed boundary method for wall-modeled large-eddy simulation of turbulent high-Mach-number flows," *J. Comput. Phys.* **470**, 111583 (2022).
- ¹⁹J.-B. Chapelier, G. Lodato, and A. Jameson, "A study on the numerical dissipation of the spectral difference method for freely decaying and wall-bounded turbulence," *Comput. Fluids* **139**, 261–280 (2016).
- ²⁰P. Stefanin Volpiani, J.-B. Chapelier, A. Schwöppe, J. Jägersküpper, and S. Champagneux, "Aircraft simulations using the new CFD software from ONERA, DLR, and Airbus," *J. Aircr.* (published online 2024).
- ²¹N. Kraiss, A. Beck, T. Bolemann, H. Frank, D. Flad, G. Gassner, F. Hindenlang, M. Hoffmann, T. Kuhn, M. Sonntag *et al.*, "Flexi: A high order discontinuous Galerkin framework for hyperbolic-parabolic conservation laws," *Comput. Math. Appl.* **81**, 186–219 (2021).
- ²²C. L. Running, B. L. Bemis, J. L. Hill, M. P. Borg, J. J. Redmond, K. Jantze, and C. Scalo, "Attenuation of hypersonic second-mode boundary-layer instability with an ultrasonically absorptive silicon-carbide foam," *Exp. Fluids* **64**, 79 (2023).
- ²³F. Bassi, L. Botti, A. Colombo, D. A. Di Pietro, and P. Tesini, "On the flexibility of agglomeration based physical space discontinuous Galerkin discretizations," *J. Comput. Phys.* **231**, 45–65 (2012).
- ²⁴F. Basile, J.-B. Chapelier, M. de la Llave Plata, R. Laraufe, and P. Frey, "Unstructured h - and hp -adaptive strategies for discontinuous Galerkin methods based on a posteriori error estimation for compressible flows," *Comput. Fluids* **233**, 105245 (2022).
- ²⁵F. Bassi and S. Rebay, "A high-order accurate discontinuous finite element method for the numerical solution of the compressible Navier–Stokes equations," *J. Comput. Phys.* **131**, 267–279 (1997).
- ²⁶F. Bassi, S. Rebay, G. Mariotti, S. Pedinotti, M. Savini *et al.*, "A high-order accurate discontinuous finite element method for inviscid and viscous turbomachinery flows," in *2nd European Conference on Turbomachinery Fluid Dynamics and Thermodynamics* (Technologisch Instituut, Antwerpen, Belgium, 1997), pp. 99–108.
- ²⁷P.-O. Persson and J. Peraire, "Sub-cell shock capturing for discontinuous Galerkin methods," AIAA Paper No. AIAA 2006-112, 2006.
- ²⁸J. Glaubitz, A. Nogueira, J. L. Almeida, R. Cantão, and C. Silva, "Smooth and compactly supported viscous sub-cell shock capturing for discontinuous Galerkin methods," *J. Sci. Comput.* **79**, 249–272 (2019).
- ²⁹F. Ducros, V. Ferrand, F. Nicoud, C. Weber, D. Darracq, C. Gacherieu, and T. Poinso, "Large-eddy simulation of the shock/turbulence interaction," *J. Comput. Phys.* **152**, 517–549 (1999).
- ³⁰C. Wang, X. Zhang, C.-W. Shu, and J. Ning, "Robust high order discontinuous Galerkin schemes for two-dimensional gaseous detonations," *J. Comput. Phys.* **231**, 653–665 (2012).
- ³¹S. Ganju, W. van Noordt, and C. Brehm, "Progress in the development of an immersed boundary viscous-wall model for 3D and high-speedflows," AIAA Paper No. AIAA 2021-0160, 2021.
- ³²C. Brehm, M. F. Barad, and C. C. Kiris, "Development of immersed boundary computational aeroacoustic prediction capabilities for open-rotor noise," *J. Comput. Phys.* **388**, 690–716 (2019).
- ³³Y. Kuya, K. Totani, and S. Kawai, "Kinetic energy and entropy preserving schemes for compressible flows by split convective forms," *J. Comput. Phys.* **375**, 823–853 (2018).
- ³⁴K. Totani, Y. Kuya, and S. Kawai, "High-order-accurate kinetic energy and entropy preserving schemes on curvilinear meshes," AIAA Paper No. AIAA 2019-1403, 2019.
- ³⁵I. Z. Reguly, G. R. Mudalige, M. B. Giles, D. Curran, and S. McIntosh-Smith, *The OPS Domain Specific Abstraction for Multi-Block Structured Grid Computations* (IEEE Press, 2014), pp. 58–67.
- ³⁶G. Coppola, F. Capuano, S. Pirozzoli, and L. de Luca, "Numerically stable formulations of convective terms for turbulent compressible flows," *J. Comput. Phys.* **382**, 86–104 (2019).
- ³⁷M. H. Carpenter and C. A. Kennedy, "Fourth-order 2N-storage Runge-Kutta schemes," Report No. NASA-TM-109112 (NASA Langley Research Center, 1994).
- ³⁸A. Hamzehloo, D. J. Lusher, S. Laizet, and N. D. Sandham, "On the performance of WENO/TENO schemes to resolve turbulence in DNS/LES of high-speed compressible flows," *Int. J. Numer. Methods Fluids* **93**, 176–196 (2021).
- ³⁹A. Babucke, *Direct Numerical Simulation of Noise-Generation Mechanisms in the Mixing Layer of a Jet* (Verlag Dr. Hut, 2009).
- ⁴⁰M. A. Keller and M. J. Kloker, "Effusion cooling and flow tripping in laminar supersonic boundary-layer flow," *AIAA J.* **53**, 902–919 (2015).
- ⁴¹M. R. Visbal and D. V. Gaitonde, "On the use of higher-order finite-difference schemes on curvilinear and deforming meshes," *J. Comput. Phys.* **181**, 155–185 (2002).
- ⁴²Y. Sun, Z. Wang, and Y. Liu, "High-order multidomain spectral difference method for the Navier-Stokes equations on unstructured hexahedral grids," *Commun. Comput. Phys.* **2**, 310–333 (2007), see http://global-sci.org/intro/article_detail/cicp/7908.html.
- ⁴³A. Jameson, "A proof of the stability of the spectral difference method for all orders of accuracy," *J. Sci. Comput.* **45**, 348–358 (2010).
- ⁴⁴P. Roe, "Approximate Riemann solvers, parameter vectors, and difference schemes," *J. Comput. Phys.* **43**, 357–372 (1981).
- ⁴⁵A. Harten and J. M. Hyman, "Self adjusting grid methods for one-dimensional hyperbolic conservation laws," *J. Comput. Phys.* **50**, 235–269 (1983).
- ⁴⁶M. Pelanti, L. Quartapelle, and L. Vigeveno, "A review of entropy fixes as applied to Roe's linearization," in *Teaching Material of the Aerospace and Aeronautics Department of Politecnico di Milano* (Politecnico di Milano, 2001), Vol. 31.
- ⁴⁷S. Gottlieb and C. Shu, "Total variation diminishing Runge-Kutta schemes," *Math. Comput.* **67**, 73–85 (1998).
- ⁴⁸G. Lodato, "Characteristic modal shock detection for discontinuous finite element methods," *Comput. Fluids* **179**, 309–333 (2019).
- ⁴⁹P.-O. Persson, "Shock capturing for high-order discontinuous Galerkin simulation of transient flow problems," AIAA Paper No. 2013-3061, 2013.
- ⁵⁰N. Tonicello, G. Lodato, and L. Vervisch, "Analysis of high-order explicit LES dynamic modeling applied to airfoil flows," *Flow, Turbul. Combust.* **108**, 77–104 (2022).
- ⁵¹X. Zhang and C.-W. Shu, "On positivity-preserving high order discontinuous Galerkin schemes for compressible Euler equations on rectangular meshes," *J. Comput. Phys.* **229**, 8918–8934 (2010).
- ⁵²See <https://github.com/flexi-framework> for the repository hosting the FLEXI software suite.
- ⁵³A. D. Beck, T. Bolemann, D. Flad, H. Frank, G. J. Gassner, F. Hindenlang, and C.-D. Munz, "High-order discontinuous Galerkin spectral element methods for transitional and turbulent flow simulations," *Int. J. Numer. Methods Fluids* **76**, 522–548 (2014).
- ⁵⁴<https://github.com/flexi-framework/hopr> for the high-order pre-processor HOPR.
- ⁵⁵M. Blind, M. Gao, D. Kempf, P. Kopper, M. Kurz, A. Schwarz, and A. Beck, "Towards exascale CFD simulations using the discontinuous Galerkin solver FLEXI," *arXiv:2306.12891* (2023).
- ⁵⁶B. Van Leer, "Towards the ultimate conservative difference scheme. IV. A new approach to numerical convection," *J. Comput. Phys.* **23**, 276–299 (1977).
- ⁵⁷P. Mossier, A. Beck, and C.-D. Munz, "A p-adaptive discontinuous Galerkin method with hp-shock capturing," *J. Sci. Comput.* **91**, 4 (2022).
- ⁵⁸C. Mavriplis, "A posteriori error estimators for adaptive spectral element techniques," in *Proceedings of the Eighth GAMM-Conference on Numerical Methods in Fluid Mechanics*, edited by P. Wesseling (Vieweg+Teubner Verlag, Wiesbaden, 1990), pp. 333–342.
- ⁵⁹M. Sonntag and C.-D. Munz, "Efficient parallelization of a shock capturing for discontinuous Galerkin methods using finite volume sub-cells," *J. Sci. Comput.* **70**, 1262–1289 (2017).
- ⁶⁰P. Mossier, D. Appel, A. D. Beck, and C.-D. Munz, "An efficient hp-adaptive strategy for a level-set ghost-fluid method," *J. Sci. Comput.* **97**, 50 (2023).
- ⁶¹B. L. Bemis, J. L. Hill, M. P. Borg, J. J. Redmond, M. Ruggeri, K. Jantze, C. Scalo, and C. L. Running, "Effect of porosity on the ability of silicon-carbide foams to attenuate second-mode boundary-layer instability," AIAA Paper No. AIAA 2023-3706, 2023.
- ⁶²B. L. Bemis, J. L. Brun, C. T. Wanstall, J. J. Hill, M. P. Borg, J. J. Redmond, M. Ruggeri, K. Jantze, C. Scalo, and C. L. Running, "Ultrasonically absorptive silicon-carbide foam for boundary-layer control" AIAA Paper No. AIAA 2023-0096, 2023.
- ⁶³M. Ruggeri, V. C. B. Sousa, and C. Scalo, "Block Spectral Stresses (BSS) estimation for shock-capturing and turbulent modeling," *arXiv:2402.19354* (2024).